

SGD with large step sizes learns sparse features

Maksym Andriushchenko

EPFL

maksym.andriushchenko@epfl.ch

Aditya Varre

EPFL

aditya.varre@epfl.ch

Loucas Pillaud-Vivien

EPFL

loucas.pillaud-vivien@epfl.ch

Nicolas Flammarion

EPFL

nicolas.flammarion@epfl.ch

Abstract

We showcase important features of the dynamics of the Stochastic Gradient Descent (SGD) in the training of neural networks. We present empirical observations that commonly used large step sizes (i) lead the iterates to jump from one side of a valley to the other causing *loss stabilization*, and (ii) this stabilization induces a hidden stochastic dynamics orthogonal to the bouncing directions that *biases it implicitly* toward simple predictors. Furthermore, we show empirically that the longer large step sizes keep SGD high in the loss landscape valleys, the better the implicit regularization can operate and find sparse representations. Notably, no explicit regularization is used so that the regularization effect comes solely from the SGD training dynamics influenced by the step size schedule. Therefore, these observations unveil how, through the step size schedules, both gradient and noise drive together the SGD dynamics through the loss landscape of neural networks. We justify these findings theoretically through the study of simple neural network models as well as qualitative arguments inspired from stochastic processes. Finally, this analysis allows to shed a new light on some common practice and observed phenomena when training neural networks. The code of our experiments is available at <https://github.com/tml-epfl/sgd-sparse-features>.

1 Introduction

During the last decade, deep neural networks have accomplished remarkable achievements on a wide variety of tasks. Yet, the understanding of their remarkable effectiveness remains incomplete. From an optimization perspective, stochastic training procedures challenge every knowledge theoreticians have drawn from convex models. In particular, large step-size schedules used in practice lead to unexpected patterns of stabilizations and sudden drops in the training loss profile. From a generalization perspective, overparametrized deep networks generalize well while fitting perfectly the data and without any explicit regularization (Zhang et al., 2017). These surprising facts suggest that optimization and generalization are tightly intertwined: neural networks find solutions that generalize well *thanks* to the optimization procedure used to train them. This property, known as *implicit bias* or *algorithmic regularization*, has been studied recently both in the case of regression (Soudry et al., 2018; Woodworth et al., 2020) and classification (Lyu and Li, 2020; Chizat and Bach, 2020; Ji and Telgarsky, 2020). However, in all these theoretical results, typical timescales needed to enter the beneficial feature learning regimes are prohibitively long and therefore may not fully capture the practical training setup.

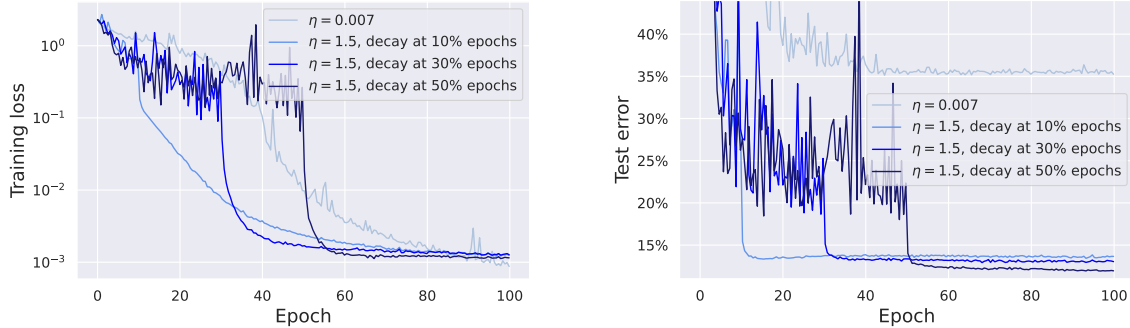


Figure 1: A typical training dynamics for a ResNet-18 trained on CIFAR-10. We use weight decay but no momentum or data augmentation for this experiment. We see a substantial difference in generalization (as large as 12% vs. 35% test error) depending on the step size η and its schedule. When the training loss stabilizes, there is a hidden progress occurring which we aim to characterize.

In this paper, we aim at staying closer to the experimental practice. Specifically, we propose to understand stochastic gradient descent (SGD) with *large step-size* schedules as introduced in the original ResNet paper (He et al., 2016) where it is first kept constant to a large value and then decayed (potentially multiple times). We illustrate this behavior in Fig. 1 where we reproduce a minimal setting with no data augmentation, momentum, and only one decrease of the step size. We draw attention to two important observations (a) the loss stays approximately constant when the step size is large and (b) despite no progress on the training loss, running this phase for longer leads to better generalization. We refer to such large step-size phase as *loss stabilization*. Our main contribution is to unveil the hidden dynamics behind this phase: loss stabilization fosters the exploration of SGD in the loss landscape and enables the model to learn *sparse features*.

1.1 Our contribution

SGD is GD + specific label noise. Noise seems to play a role of paramount importance to help the training dynamics travel the loss landscape (Keskar et al., 2016; Xing et al., 2018). There have been attempts to highlight this property by studying stochastic differential equations (SDEs), but this approach has not been completely satisfactory since the noise covariance is rarely well understood. We show here that SGD can be cast exactly as GD with a specific label noise that scales with the training loss. This allows to unveil the specific shape and scale of the SGD noise allowing to model it in a suitable SDE.

Large step sizes SGD enables exploration by loss stabilization. On the one hand, we show that loss stabilization is not due to a saddle-to-saddle behavior (Jacot et al., 2021; Barak et al., 2022) but rather to bouncing side-to-side above some valley and where sudden drops occur when the step size is lowered. We model it as a fast-slow dynamics where (i) the fast movement is determined by the bouncing directions causing loss stabilization (ii) the slow dynamics drives SGD to explore efficiently the loss landscape by the combination of the gradient and multiplicative noise.

Exploration leads SGD to learn sparse features. The hidden slow dynamics during loss stabilization is showcased as an SDE whose multiplicative noise is related to the neural tangent

kernel features. We show in a simple model (diagonal linear networks) that this multiplicative noise structure leads SGD to learn sparse features. Building on this, we conjecture a similar effect for more complicated architectures and experimentally show it on neural networks of increasing complexity. We demonstrate how the loss stabilization phase is crucial to ensure that convergence does not occur too early to suboptimal near predictors, hence showing the benefit from the hidden dynamics of SGD.

Insights from our understanding. Overall, we observe a clear general picture: the hidden optimization dynamics induced by large step sizes and loss stabilization allows to exit from the lazy regime (Chizat et al., 2019) and rapidly transition to a sparse feature learning regime. We shed a new light on phenomena observed in practice and give a sense on when the exploration and fitting phases happen. We argue that after a short initial phase of training, SGD *first* tends to learn sparse feature of the signal *and then eventually* fits it when the step size is decayed enough. Finally, we discuss informally how many deep learning regularization methods (weight decay, BatchNorm, SAM) also fit into the same picture.

1.2 Related work

He et al. (2016) popularized the piecewise constant step-size schedule which often exhibits a clear loss stabilization pattern. However, they did not provide any explanations for such training dynamics and its implicit regularization effect. Non-monotonic patterns of the training loss have been explored in recent works. We emphasize that the loss stabilization we consider is different (i) from the catapult mechanism (Lewkowycz et al., 2020) where no stabilization occurs, and (ii) from the *spiked* convergence regime described in the edge of stability paper (Cohen et al., 2021) as we consider an even larger step-size regime.

Past works conjectured that large step sizes induce the minimization of some hidden complexity measures related to flatness of minima (Keskar et al., 2016; Smith and Le, 2018). Notably, Xing et al. (2018) point out that SGD moves through the loss landscape bouncing between the walls of a valley where the role of the step size is to guide exploration of SGD towards a flatter minimum. However, many typically used flatness definitions are questionable for this purpose (Dinh et al., 2017) and there is no clear conclusion about the hidden complexity measure and its properties. For example, full-batch gradient descent with large step sizes (unlike SGD) leads to flat solutions which are not well-generalizing (Kaur et al., 2022). Note that it is possible to bridge the gap between GD and SGD by using explicit regularization as in Geiping et al. (2022). We instead focus on the *implicit* regularization of SGD which remains the most practical approach for training deep networks.

The importance of large step sizes has been investigated with diverse motivations. However, we believe that existing approaches do not sufficiently capture the *hidden stochastic dynamics* behind the loss stabilization phenomenon observed for deep networks. Attempts to explain it on strongly convex models (Nakkiran, 2020; Wu et al., 2021; Beugnot et al., 2022) are inherently incomplete since it is a phenomenon related to the existence of many zero solutions with very different generalization properties. Li et al. (2019b) analyzed the role of loss stabilization for a synthetic distribution containing different patterns, but it is not clear how this analysis can be extended to general problems. Works based on stability analysis characterize the properties of the minimum that SGD or GD can potentially converge depending on the step size (Wu et al., 2018; Mulayoff et al., 2021; Ma and Ying, 2021; Nacson et al., 2022). However, these approaches *do not capture the entire training dynamics* which is important as for the training schedules we consider,

SGD converges only after we switch from large to small step sizes. SGD with label noise has been studied because of its beneficial regularization effect and its resemblance to SGD’s standard noise. Its implicit bias has been first characterized by [Blanc et al. \(2020\)](#) and extended by [Li et al. \(2022\)](#). However, their analysis only holds in the final phase of the training, close to a zero-loss manifold. Our work instead is closer in spirit to [Pillaud-Vivien et al. \(2022\)](#) where the label noise dynamics is analyzed in the *central* phase of the training.

Finally, sparse features and low-rank structures in deep networks have been commonly used for model compression, knowledge distillation, and lottery ticket hypothesis ([Denton et al., 2014](#); [Hinton et al., 2015](#); [Frankle and Carbin, 2018](#)). A common theme of all these works is the presence of *hidden structure* in the networks learned by SGD which allows one to come up with a much smaller network that approximates well the original one. In particular, [Hoefer et al. \(2021\)](#) note that ReLU activations in deep networks trained with SGD are typically much sparser than 50%. Our findings suggest that the step size schedule can be the key component behind emergence of such sparsity.

2 The effective dynamics of SGD with large step-size: sparse feature learning

In this section, we show that large step sizes lead the loss to stabilize by making SGD bounce above a valley. We then unveil the effective dynamics induced by this loss stabilization. To clarify our exposition we showcase our results for the mean square error but other losses like the cross-entropy carry the same properties ([Wojtowytsch, 2021b](#)). We consider a generic parameterized family of prediction functions $\mathcal{H} := \{x \rightarrow h_\theta(x), \theta \in \mathbb{R}^p\}$, a setting which encompasses neural networks. In this case, the training loss on input/output samples $(x_i, y_i)_{1 \leq i \leq n} \in \mathbb{R}^d \times \mathbb{R}$ reads

$$\mathcal{L}(\theta) := \frac{1}{2n} \sum_{i=1}^n (h_\theta(x_i) - y_i)^2. \quad (1)$$

We consider the overparameterized setting, i.e. $p \gg n$, hence, there shall exists many parameters θ^* that lead to zero loss, i.e., perfectly interpolate the dataset. Therefore, the question of which interpolator the algorithm converges to is of paramount importance in terms of generalization: as said in the introduction, we refer it as the *implicit bias* of the algorithm. We focus on the SGD recursion with step size $\eta > 0$, initialized at $\theta_0 \in \mathbb{R}^p$: for all $t \in \mathbb{N}$,

$$\theta_{t+1} = \theta_t - \eta(h_{\theta_t}(x_{i_t}) - y_{i_t}) \nabla_\theta h_{\theta_t}(x_{i_t}), \quad (2)$$

where $i_t \sim \mathcal{U}(\llbracket 1, n \rrbracket)$ is the uniform distribution over the sample indexes. In the following, note that considering SGD with mini batches of size B would lead to similar analysis (replacing η by η/B).

2.1 SGD is GD with specific label noise

To put emphasis on the combined roles of gradient and noise, we draw the connection between the SGD dynamics and that of full-batch GD where we add a specific noise to the labels at each iteration.

Proposition 1. Let $(\theta_t)_{t \geq 0}$ follows the SGD dynamics Eq.(2) with sampling function $(i_t)_{t \geq 0}$. Define for each $t \geq 0$, the random vector $\xi_t \in \mathbb{R}^n$ such that for all $i \in \llbracket 1, n \rrbracket$,

$$[\xi_t]_i := (h_{\theta_t}(x_i) - y_i)(1 - n\mathbf{1}_{i=i_t}). \quad (3)$$

Then, $(\theta_t)_{t \geq 0}$ follows the dynamics of the full-batch gradient dynamics on \mathcal{L} where at each iteration $t \geq 0$ we inject noise ξ_t to the label vector $y \in \mathbb{R}^n$: that is at step $t \geq 0$, we compute the gradient of \mathcal{L} considering the random labels $y_t := y + \xi_t$.

This proposition links the dynamics of SGD to the one of GD plus a certain amount of label noise. The scale of this induced noise is characterized in the following lemma. Refer to App. A for the proofs.

Lemma 2. For $t \geq 0$, let $\xi_t \in \mathbb{R}^n$ be defined as in Proposition 1, then ξ_t is a mean zero random vector with variance such that $\frac{1}{n(n-1)}\mathbb{E}\|\xi_t\|^2 = 2\mathcal{L}(\theta_t)$.

Hence, the effective label noise decays with the training loss. The effect of the SGD noise therefore decreases during the optimization process. However, we highlight in the following section that the loss can stabilize because of large step sizes which makes the amount of label noise constant. This feature enables to unveil the effective dynamics that take place during loss stabilization.

2.2 The effective dynamics behind loss stabilization

On loss stabilization. For generic quadratic costs, e.g., $F(\beta) := \|X\beta - y\|^2$, gradient descent with step size η is convergent for $\eta < 2/\lambda_{\max}$, divergent for $\eta > 2/\lambda_{\max}$ and converges to a bouncing 2-periodic dynamics for $\eta = 2/\lambda_{\max}$, where λ_{\max} is the largest eigenvalue of the Hessian. However, the practitioner is not likely to hit perfectly this unstable step size and, almost surely, the dynamics shall either converge or diverge. Yet, non-quadratic costs bring to this picture a particular complexity: it has been shown that, even for non-convex toy models, there exist an open interval of step sizes for which the gradient descent neither converge nor diverge (Ma et al., 2022; Chen and Bruna, 2022). As we are interested in SGD, we complement this result by presenting a toy example in which loss stabilization occurs almost surely *in the case stochastic updates*. Indeed, consider a regression problem with quadratic parameterization on one-dimensional data inputs x_i 's, coming from a distribution $\hat{\rho}$, and outputs generated by the linear model $y_i = x_i\theta_*^2$. The loss writes $F(\theta) := \frac{1}{4}\mathbb{E}_{\hat{\rho}}(y - x\theta^2)^2$, and the SGD iterates with step size $\eta > 0$ follow, for any $t \in \mathbb{N}$,

$$\theta_{t+1} = \theta_t + \eta \theta_t x_{i_t} (y_{i_t} - x_{i_t} \theta_t^2) \quad \text{where} \quad x_{i_t} \sim \hat{\rho}. \quad (4)$$

For the sake of concreteness and clarity, suppose that $\theta_* = 1$ and $\text{supp}(\hat{\rho}) = [a, b]$, we have the following proposition (a more general result can be found in Proposition 7 of the Appendix).

Proposition 3. For any $\eta \in (a^{-2}, 1.25 \cdot b^{-2})$ and initialization $\theta_0 \in (0, 1)$, for $t > 0$,

$$\delta_1 < F(\theta_t) < \delta_2 \quad \text{almost surely, and} \quad (5)$$

$$\exists T > 0, \forall k > T, \quad \theta_{t+2k} < 1 < \theta_{t+2k+1} \quad \text{almost surely.} \quad (6)$$

where $\delta_1, \delta_2, T > 0$ are constant given in the Appendix.

The proposition is divided in two parts: for some range of step sizes, Eq.(5) shows that the loss stabilizes in between level sets δ_1 and δ_2 and Eq.(6) shows that after some initial phase, the iterates bounce from one side of the *loss valley* to the other one. Note that despite the stochasticity of the procedure, the results hold *almost surely*.

The effective dynamics. As observed in the prototypical SGD training dynamics of Fig. 1 and proved in the non-convex toy model of Proposition 3, large step sizes lead the loss to stabilize around some level set. To further understand the effect of this loss stabilization in parameter space, we shall assume perfect stabilization and thus that the loss $L(\theta_t)$ remains equal to some constant. Then, from Proposition 1, that links SGD with GD plus label noise, and Lemma 2, that shows that the noise scales like the loss, we infer the following claim.

Claim 4. *During loss stabilization, SGD is well modelled by GD with constant label noise.*

Label noise dynamics have been studied recently (Blanc et al., 2020; Damian et al., 2021; Li et al., 2022) thanks to their connection with continuous time Stochastic Differential Equations (SDEs). To properly write a SDE model, the drift should match the gradient descent and the noise should have the correct covariance structure (Li et al., 2019a; Wojtowytch, 2021a). Claim 4 implies that the noise at state θ is spanned by the gradient vectors $\{\nabla_\theta h_\theta(x_1), \dots, \nabla_\theta h_\theta(x_n)\}$ and has a constant intensity corresponding to the loss stabilization at a level $\delta > 0$. Hence, we propose the following SDE model

$$d\theta_t = -\nabla_\theta \mathcal{L}(\theta_t) dt + \sqrt{\eta\delta} \phi_{\theta_t}(X)^\top dB_t, \quad (7)$$

where $(B_t)_{t \geq 0}$ is a standard Brownian motion in \mathbb{R}^n and we will refer to $\phi_\theta(X) := [\nabla_\theta h_\theta(x_i)^\top]_{i=1}^n \in \mathbb{R}^{n \times p}$ as the *Neural Tangent Kernel (NTK) feature matrix* (Jacot et al., 2018). This SDE can be seen as *the effective slow dynamics* that drives the iterates while they bounce *rapidly* in some directions at the level set δ (fast dynamics). It highlights the combination of the deterministic part of the full-batch gradient and the noise induced by SGD at level set δ . In the next section, we leverage the SDE (7) to understand the implicit bias of such learning dynamics.

2.3 Sparse feature learning

In this section, we give insights on the effective dynamics given by Eq.(7). We begin with a simple model of diagonal linear networks that showcase a sparse-inducing dynamics and further disclose our general message about the overall implicit bias promoted by the effective dynamics.

2.3.1 A warm-up: diagonal linear networks

An appealing example of simple non-linear networks that help in forging an intuition for more complicated architectures are diagonal linear networks (Vaskevicius et al., 2019; Woodworth et al., 2020; HaoChen et al., 2021; Pesme et al., 2021). They are two-layer linear networks with only diagonal connections: the prediction function writes $h_{u,v}(x) = \langle u, v \odot x \rangle = \langle u \odot v, x \rangle$ where \odot denotes *elementwise* multiplication. Even though the loss is convex in the associated linear predictor $\beta := u \odot v \in \mathbb{R}^d$, it is not in (u, v) , hence the training of such simple models already exhibit a rich non-convex dynamics. In this case, $\nabla_u h_{u,v}(x) = v \odot x$, and the SDE model Eq.(7) writes

$$du_t = -\frac{1}{n} [X^\top (X(u_t \odot v_t) - y)] \odot v_t dt + \sqrt{\eta\delta} v_t \odot [X^\top dB_t], \quad (8)$$

where $(B_t)_{t \geq 0}$ is a standard Brownian motion in \mathbb{R}^n . Equations are symmetric for $(v_t)_{t \geq 0}$.

What is the behaviour of this effective dynamics? [Pillaud-Vivien et al. \(2022\)](#) answered this question by analyzing a similar stochastic dynamics and unveiled the sparse nature of the resulting solutions. Indeed, under sparse recovery assumptions, denoting β^* the sparsest linear predictor that interpolates the data, it is shown that the associated linear predictor $\beta_t = u_t \odot v_t$: (i) converges exponentially fast to zero outside of the support of β^* (ii) is *with high probability* in a $\mathcal{O}(\sqrt{\eta\delta})$ neighborhood of β^* in its support after a time $\mathcal{O}(\delta^{-1})$.

Overall conclusion on the model. During a first phase, SGD with large step sizes η decreases the train loss until stabilization at some level set $\delta > 0$. During this loss stabilization, an effective noise-driven dynamics takes place. It shrinks the coordinates outside of the support of the sparsest signal and oscillates in parameter space at level $\mathcal{O}(\sqrt{\eta\delta})$ on its support. Hence, decreasing later the step size leads to perfect recovery of the sparsest predictor. This behaviour is illustrated in our experiments in Figure 2.

2.3.2 The sparse feature learning conjecture for more general models

Results for diagonal linear nets recalled in the previous paragraph show that the noisy dynamics (8) induce a *sparsity bias*. As emphasized in [HaoChen et al. \(2021\)](#), this effect is largely due to the multiplicative structure of the noise $v \odot [X^\top dB_t]$ that, in this case, has a shrinking effect *on the coordinates* (because of the coordinate-wise multiplication with v). In the general case, we see, thanks to Eq.(7), that the same multiplicative structure of the noise still happens but this time *with respect to the NTK feature matrix $\phi_\theta(X)$* . Hence, this suggests that similarly to the diagonal linear network case, the implicit bias of the noise can lead to a shrinkage effect applied to $\phi_\theta(X)$. Remarkably, from a stability perspective, [Blanc et al. \(2020\)](#) showed that the SGD dynamics implicitly tries to minimize the *Frobenius norm* $\|\phi_\theta(X)\|_{\text{F}} = \sum_{i=1}^n \|\nabla_\theta h_\theta(x_i)\|^2$. However, building on [Pillaud-Vivien et al. \(2022\)](#), when noise is too high, it seems that the multiplicative factor has a stronger effect: it drives each direction to the lowest norm. Indeed, an interesting property of Brownian motion is that, for $v \in \mathbb{R}^p$, $\langle v, B_t \rangle = \|v\|_2 W_t$, where the equality is valid in law and $(W_t)_{t \geq 0}$ is a one-dimensional Brownian motion. Hence, this suggests that

*The noise part of Eq.(7) tries to minimize the ℓ_2 -norm of **each column** of $\phi_\theta(X)$.*

Note that we put **each** in emphasis to stress on the difference with the sum structure of the Frobenius norm. Also note that the *fitting part* of the dynamics prevents the NTK feature matrix to collapse totally to zero, but as soon as they are not needed to fit the signal, *columns* can be reduced to zero. We provide below a specification of this implicit bias for different architectures:

- **Diagonal linear networks:** For $h_{u,v}(x) = \langle u \odot v, x \rangle$, we have $\nabla_{u,v} h_{u,v}(x) = [v \odot x, u \odot x]$. Thus, for a generic data matrix X , minimizing the norm of each column of $\phi_{u,v}(X)$ amounts to put the maximum of zero coordinates and hence to minimize $\|u \odot v\|_0$.
- **ReLU networks:** We take the prototypical one hidden layer to exhibit the sparsification effect. Let $h_{a,W}(x) = \langle a, \sigma(Wx) \rangle$, then $\nabla_a h_{a,W}(x) = \sigma(Wx)$ and $\nabla_{w_j} h_{a,W}(x) = a_j x \mathbf{1}_{\langle w_j, x \rangle > 0}$. Note that the ℓ_2 -norm of the column corresponding to the neuron is reduced when it is activated at a *minimal number of training points*, hence the implicit bias enables the learning of *sparse data-active features*. Finally, when some directions are needed to fit the data, similarly activated neurons align to fit, allowing the rank of $\phi_\theta(X)$ to be also a good proxy for this feature sparsity.

Overall, fully understanding theoretically the structural implications of the implicit bias described above remains an exciting avenue for future work. We show next that the conjectured sparsity is indeed observed empirically for a variety of models, as well as that the rank reduction of $\phi_\theta(X)$ can be used as a good proxy of the hidden progress of the loss stabilization phase.

3 Empirical evidence of sparse feature learning driven by SGD

Here we present empirical results¹ for neural networks of increasing complexity: from diagonal linear networks to deep residual networks on CIFAR-10 and CIFAR-100. We make the following common observations for all these networks trained using SGD schedules with large step sizes:

- (O1) **Loss stabilization:** training loss stabilizes around a high level set until step size is decayed,
- (O2) **Generalization benefit:** longer loss stabilization leads to better generalization,
- (O3) **Sparse feature learning:** longer loss stabilization leads to sparser features.

Importantly, *we use no explicit regularization* in our experiments so that the training dynamics is driven purely by SGD and the step size schedule. Additionally, in some cases, we cannot find a single large step size that would lead to loss stabilization. In such cases, whenever explicitly mentioned, we use a *warmup* step size schedule—i.e., increasing step sizes according to some schedule—to make sure that the training loss stabilizes around some level set. Such warmup schedules are commonly used in practice (He et al., 2016; Devlin et al., 2018). Warmup is often motivated purely from the optimization perspective as a way to accelerate training (Agarwal et al., 2021) but we claim that, more importantly, it as a way to enhance the implicit regularization effect of SGD.

Measuring sparse feature learning. Our main insight is that the NTK feature matrix is significantly simplified in the loss stabilization phase, and that the rank of $\phi_\theta(X)$ (i.e., the sparsity of its singular values) is a good proxy to track this dynamics. We compute it over iterations for each model (except deep networks where it is not feasible) by using a fixed threshold on the singular values of $\phi_\theta(X)$ normalized by the largest singular value. In this way, we ensure that the difference in the rank that we detect is not simply due to a different scales of $\phi_\theta(X)$. Moreover, we always compute $\phi_\theta(X)$ on the number of fresh samples equal to the number of parameters $|\theta|$ to make sure that rank deficiency is not coming from a small value of $n \ll |\theta|$ which is the case in the overparametrized settings we consider.

Furthermore, we also want to track a more direct and interpretable notion of feature sparsity. This motivates us to count the average number of *distinct* (i.e., counting a group of highly correlated activations as one), *non-zero* activations at some layer over the training set which we refer to as the *feature sparsity coefficient*. We count a pair of activations i and j as highly correlated if their Pearson’s correlation coefficient—i.e., $C_{ij}/\sqrt{C_{ii}C_{jj}}$ where C is the covariance matrix computed over the training samples—is at least 0.95. Unlike $\text{rank}(\phi_\theta(X))$, the feature sparsity coefficient scales to deep networks and has an easy-to-grasp meaning.

3.1 Sparse feature learning in diagonal linear networks

Setup. The inputs x_1, \dots, x_n with $n = 80$ are sampled from $\mathcal{N}(0, \mathbf{I}_d)$ where \mathbf{I}_d is an identity matrix with $d = 200$, and the outputs are generated as $y_i = \langle \beta_*, x_i \rangle$ where $\beta_* \in \mathbb{R}^d$ is $r = 20$ sparse.

¹The code of all our experiments is available at <https://github.com/tml-epfl/sgd-sparse-features>.

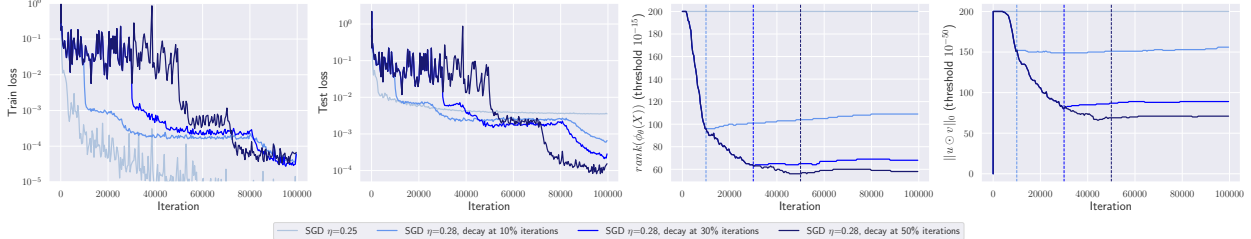


Figure 2: Diagonal linear networks. We observe loss stabilization, better generalization for longer schedules, minimization of the rank of $\phi_\theta(X)$ and sparsity of the predictor $u \odot v$.

We consider four different SGD runs (started from $u_i = 0.1$, $v_i = 0$ for each i): one with a small step size and three other with initial large step size decayed after 10%, 30%, 50% iterations, respectively.

Observations. We show the results in Fig. 2 and note that **(O1)–(O3)** hold even in this simple model trained with vanilla SGD without any explicit regularization or layer normalization schemes. We observe that the training loss stabilizes around $10^{-1.5}$, the test loss improves for longer schedules, both $\text{rank}(\phi_\theta(X))$ and $\|u \odot v\|_0$ decrease during the loss stabilization phase leading to a sparse final predictor. While the training loss has seemingly converged to $10^{-1.5}$, a hidden dynamics suggested by Eq.(8) occurs which slowly drifts the iterates to a sparse solution. This implicit sparsification explains the dependence of the final test loss on the time when the large step size is decayed, similarly to what has been observed for deep networks in Fig. 1. Interestingly, we also note that SGD with large step-size schedules encounters saddle points *after* we decay the step size (see the training loss curves in Fig. 2) which resembles the saddle-to-saddle regime described in [Jacot et al. \(2021\)](#) which does not occur in the large-initialization lazy training regime.

SGD and GD have different implicit biases. Since we observe from Fig. 2 that for loss stabilization, stochasticity alone does not suffice and large step sizes are necessary, one may wonder if conversely only large step sizes can be sufficient to have a sparsifying effect. Even if special instances can be found for which large step sizes are sufficient ([Nacson et al., 2022](#)), we answer this negatively showing that gradient descent in general does not go to the sparsest solution as demonstrated in Fig. 8 in the Appendix. Moreover, in Fig. 3, we visualize the difference in trajectory between the two methods taken with large step sizes over a 2D subspace spanned by $w^* - w_{init}$ and $w_{flow} - w_{init}$, where w^* is the ground truth, w_{flow} is the result of gradient flow, and w_{init} is the initialization. This example provides an important intuition that loss stabilization alone is not sufficient for sparsification and that the role of noise described earlier is crucial.

3.2 Sparse feature learning in simple ReLU networks

Two-layer ReLU network in 1D. We consider the one-dimensional regression task from [Blanc et al. \(2020\)](#) with 12 points, where label noise SGD has been shown to learn a simple model. We show that similar results can be achieved with large-step-size SGD via loss stabilization. We train

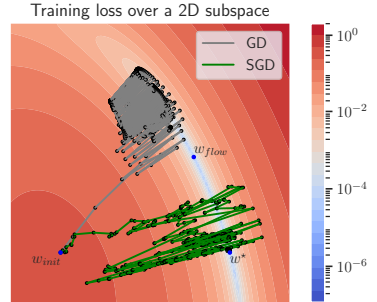


Figure 3: GD and SGD take different trajectories.

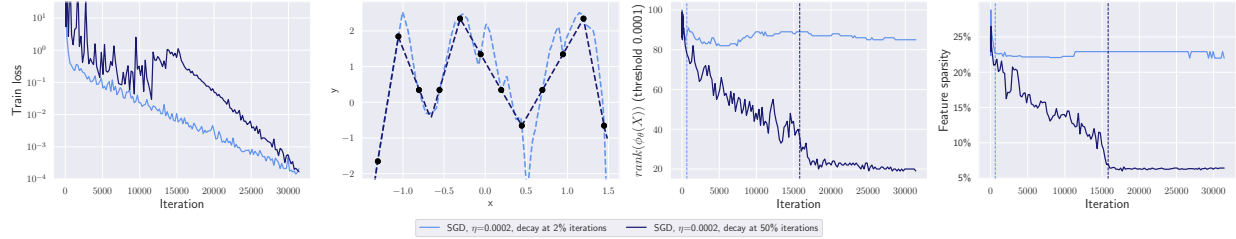


Figure 4: Two-layer ReLU networks for 1D regression. We observe loss stabilization, simplification of the model trained with a longer schedule, lower rank of $\phi_\theta(X)$, and much sparser features.

a ReLU network with 100 neurons with SGD with a linear warmup (otherwise, we were unable to achieve approximate loss stabilization), directly followed by a step-size decay. The two plots correspond to a warmup/decay transition at 2% and 50% of iterations, respectively. The results shown in Fig. 4 confirm that **(O1)–(O3)** hold: the training loss stabilizes around $10^{-0.5}$, the predictor becomes much simpler and is expected to generalize better, and both $\text{rank}(\phi_\theta(X))$ and the feature sparsity coefficient substantially decrease during the loss stabilization phase. For this one-dimensional task, we can directly observe the final predictor which is sparse in terms of the number of distinct ReLU kinks as captured by the feature sparsity coefficient and the rank of the NTK feature matrix. Interestingly, we also observed *overregularization* for even larger step sizes when we cannot fit all the training points (see Fig. 9 in Appendix). This phenomenon clearly illustrates how the capacity control is induced by the optimization algorithm: *the function class over which we optimize depends on the step size schedule*. Additionally, Fig. 10 in Appendix shows the evolution of the predictor over iterations. The general picture is confirmed: first the model is simplified during the loss stabilization phase and only then fits the training data.

Illustration of neuron dynamics. We illustrate the change of neurons during training of two-layer ReLU networks in the teacher-student setup of Chizat et al. (2019) (see Fig. 1 therein) using a large initialization scale for which small step sizes of GD or SGD lead to lazy training. We postpone the illustration of **(O1)–(O3)** to Fig. 11 in Appendix as our interest is on showing neuron dynamics (Fig. 5). We see that for SGD with a small step size, the neurons w_i stay close to their initialization, while for a large step size, there is a clear clustering of directions w_i along the teacher directions w_i^* . The overall picture is very similar to Fig. 1 of Chizat et al. (2019) where the same feature learning effect is achieved via gradient flow from a small initialization which is, however, much more computationally expensive due to the saddle point at zero. Finally, we note that the clustering phenomenon of neurons w_i motivates the removal of highly correlated activations in the feature sparsity coefficient: although the corresponding activations are often non-zero, many of them in fact implement *the same feature* and thus should be counted only once.

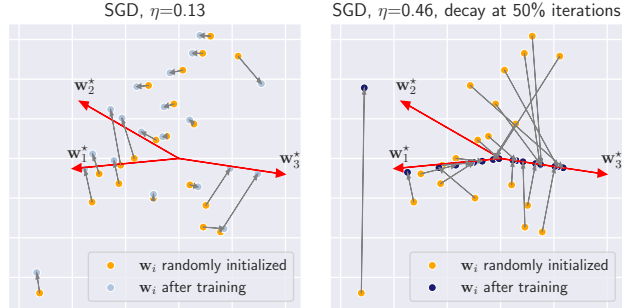


Figure 5: Only for a large step size, the neurons w_i cluster along the teacher neurons w_i^* leading to a model that uses a sparse set of features.

Finally, we note that the clustering phenomenon of neurons w_i motivates the removal of highly correlated activations in the feature sparsity coefficient: although the corresponding activations are often non-zero, many of them in fact implement *the same feature* and thus should be counted only once.

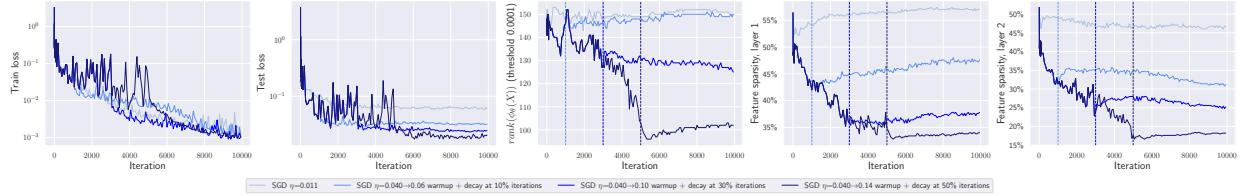


Figure 6: Three-layer ReLU networks in a teacher-student setup. Loss stabilization occurs and leads to a lower rank of the NTK feature matrix and lower feature sparsity on *both* hidden layers.

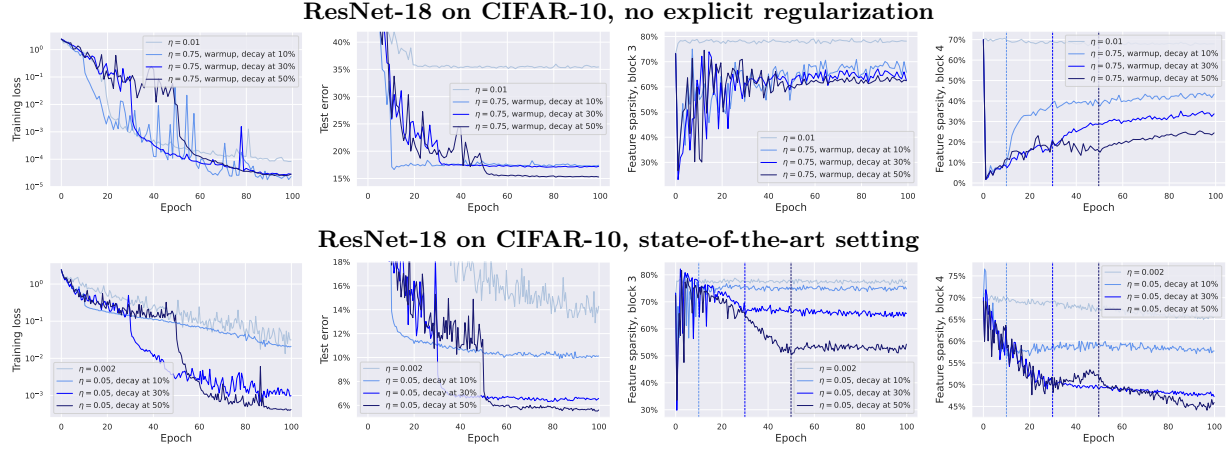


Figure 7: ResNet-18 trained on CIFAR-10. Both *without explicit regularization* and in the *state-of-the-art setting*, the training loss stabilizes, the test loss noticeably depends on the length of the schedule, and feature sparsity is minimized over iterations.

Deeper ReLU networks. We use a teacher-student setup with a random *three-layer* teacher ReLU network having 2 neurons on each hidden layer. The student network is overparametrized with 10 neurons on each layer and is trained on 50 examples. We train models using SGD with a medium constant step size and a large step size with warmup which is decayed after 10%, 30%, 50% iterations, respectively. The results shown in Fig. 6 confirm that **(O1)–(O3)** hold: the training loss stabilizes around $10^{-1.5}$, the test loss is smaller for longer schedules, and both $\text{rank}(\phi_\theta(X))$ and the feature sparsity coefficient substantially decrease during the loss stabilization phase. All methods have the same value of the training loss (10^{-3}) after 10^4 iterations but different generalization. Moreover, we see that the feature sparsity coefficient decreases *on each layer* which makes this metric a promising one to consider for deeper networks.

3.3 Sparse feature learning in deep ReLU networks

Setup. We consider here an image classification task and train a ResNet-18 and ResNet-34 on CIFAR-10 and CIFAR-100 using SGD with batch size 256 and different step size schedules. We use an exponentially increasing warmup schedule with exponent 1.05 to stabilize the training loss. We cannot measure the rank of $\phi(X)$ here since this matrix is too large ($\approx 50\,000 \times 20\,000\,000$) so we measure only the feature sparsity coefficient taken at two layers: at the end of super-block 3 (i.e., in the middle of the network) and super-block 4 (i.e., right before global average pooling in the end of the network) of ResNets. We test two settings: a basic setting without explicit regularizers

such as weight decay and a state-of-the-art setting with weight decay, momentum, and standard augmentations.

Observations. The results on CIFAR-10 shown in Fig. 7 confirm that our main findings still hold also in this setting: the training loss stabilizes either slightly below 10^{-1} or above 10^{-1} , the test error is becoming progressively better for longer schedules, as well as the feature sparsity coefficient. Small step sizes lead to bad generalization, especially without explicit regularization: 35% test error compared to 15% for large step sizes. This poor performance confirms that it is crucial to leverage the implicit bias of large step sizes. The difference in the feature sparsity coefficient is also substantial with the final model having 70% instead of 24% at block 4 without explicit regularization. The observations are similar for the state-of-the-art setting as well where even with explicit regularization, we still see a noticeable difference in generalization and feature sparsity depending on the step size and schedule. We further note that feature sparsity coefficient is gradually minimized over iterations in this case (similarly to Figures 2, 4, 6) while without explicit regularization we observe a different pattern: a very quick drop down to almost zero at the very first epoch and then a gradual increase.

We show the results with similar findings on CIFAR-100 in Fig. 13 in Appendix. Additionally, Fig. 12 illustrates that for small step sizes, the early and middle layers stay very close to their random initialization which indicates the absence of feature learning similarly to what is suggested by the neuron movement plot in Fig. 5. Finally, in Fig. 14 we additionally show feature sparsity computed at the first two super-blocks of ResNets.

4 Insights from our understanding of the training dynamics

Here we provide an extended discussion on the implications of our theoretical and empirical findings.

The multiple stages of the SGD training dynamics. As analyzed and shown empirically, deep learning training dynamics can be split onto three distinct phases: (i) an initial phase of reducing the loss down to some level where stabilization can occur, (ii) a loss stabilization phase where noise and gradient directions combine to find architecture-dependent sparse representations of the data, (iii) a final phase when the step size is decreased to fit the training data. This typology allows to clearly disentangle the effect of the exploration phase (ii) which relies on the implicit bias of SGD to simplify the model. Note that phases (ii) and (iii) can be repeated multiple times until final convergence (He et al., 2016). Moreover, in some training schedules, (ii) might not explicitly occur and the effect of loss stabilization (ii) and data fitting (iii) can occur simultaneously (Nakkiran et al., 2019).

From lazy training to feature learning. Similar sparse implicit biases have been shown for regression with infinitely small initialization (Boursier et al., 2022) and for classification (Chizat and Bach, 2020; Lyu and Li, 2020). However, both approaches are not practical from the computational point of view since (i) the origin is a saddle point for regression leading to the vanishing gradient problem (especially, for deep networks), and (ii) max-margin bias for classification is only expected to happen in the asymptotic phase (Moroshko et al., 2020). On the contrary, large step sizes enable to initialize far from the origin, while allowing to *efficiently* transition from a regime close to the

lazy NTK regime (Jacot et al., 2018) to the rich feature learning regime where the model learns sparse representations.

Common patterns in the existing techniques. Tuning the step size to obtain loss stabilization can be difficult. To prevent early divergence caused by too large step sizes, we sometimes had to rely on an increasing step size schedule (known as *warmup*). Interpreting such schedules as a tool to favor implicit regularization provides a new explanation to their success and popularity. Additionally, normalization schemes like *batch normalization* or *weight decay*, beyond carrying their own implicit or explicit regularization properties, can be analyzed from a similar lens: they allow to use larger step sizes that boost further the implicit bias effect of SGD while preventing divergence (Bjorck et al., 2018; Zhang et al., 2018). Note also that we derived our analysis with batch size equal to one for the sake of clarity, but an arbitrary batch size B would simply be equivalent to replacing $\gamma \leftarrow \gamma/B$. Similarly to the consequence of large step sizes, preferring *smaller batch sizes* (Keskar et al., 2016) while avoiding divergence seem key to benefit from the implicit bias of SGD. Finally, the effect of large step sizes or small batches is often connected to measures of *flatness* of the loss surface via stability analysis (Wu et al., 2018) and some methods like the Hessian regularization (Damian et al., 2021) or SAM (Foret et al., 2021) explicitly optimize it. Such methods resemble the implicit bias of SGD with loss stabilization implied by the label noise equation (Eq.(7)) where matrix $\phi_\theta(X)$ is the key component of the Hessian. However, an important practical difference is that the regularization strength in these methods is explicit and decoupled from the step size schedule which may be harder to properly tune since it is simultaneously responsible for optimization *and* generalization.

Acknowledgements

We thank Maria-Luiza Vladarean and Scott Pesme for insightful discussions and proofs checking. M.A. was supported by the Google Fellowship and Open Phil AI Fellowship. A.V. was supported by the Swiss Data Science Center Fellowship. L.P.V.’s work was partially supported by the Simons Foundation.

References

- N. Agarwal, S. Goel, and C. Zhang. Acceleration via fractal learning rate schedules. In International Conference on Machine Learning, pages 87–99. PMLR, 2021.
- B. Barak, B. L. Edelman, S. Goel, S. Kakade, E. Malach, and C. Zhang. Hidden progress in deep learning: Sgd learns parities near the computational limit. arXiv preprint arXiv:2207.08799, 2022.
- G. Beugnot, J. Mairal, and A. Rudi. On the benefits of large learning rates for kernel methods. arXiv preprint arXiv:2202.13733, 2022.
- N. Bjorck, C. P. Gomes, B. Selman, and K. Q. Weinberger. Understanding batch normalization. Advances in neural information processing systems, 31, 2018.
- G. Blanc, N. Gupta, G. Valiant, and P. Valiant. Implicit regularization for deep neural networks driven by an ornstein-uhlenbeck like process. In Conference on learning theory, pages 483–513. PMLR, 2020.

E. Boursier, L. Pillaud-Vivien, and N. Flammarion. Gradient flow dynamics of shallow relu networks for square loss and orthogonal inputs. [arXiv preprint arXiv:2206.00939](#), 2022.

L. Chen and J. Bruna. On gradient descent convergence beyond the edge of stability. [arXiv preprint arXiv:2206.04172](#), 2022.

L. Chizat and F. Bach. Implicit bias of gradient descent for wide two-layer neural networks trained with the logistic loss. In [Conference on Learning Theory](#), pages 1305–1338. PMLR, 2020.

L. Chizat, E. Oyallon, and F. Bach. On lazy training in differentiable programming. [Advances in Neural Information Processing Systems](#), 32, 2019.

J. M. Cohen, S. Kaur, Y. Li, J. Z. Kolter, and A. Talwalkar. Gradient descent on neural networks typically occurs at the edge of stability. [arXiv preprint arXiv:2103.00065](#), 2021.

A. Damian, T. Ma, and J. D. Lee. Label noise sgd provably prefers flat global minimizers. [Advances in Neural Information Processing Systems](#), 34:27449–27461, 2021.

E. L. Denton, W. Zaremba, J. Bruna, Y. LeCun, and R. Fergus. Exploiting linear structure within convolutional networks for efficient evaluation. [Advances in neural information processing systems](#), 27, 2014.

J. Devlin, M.-W. Chang, K. Lee, and K. Toutanova. Bert: Pre-training of deep bidirectional transformers for language understanding. [arXiv preprint arXiv:1810.04805](#), 2018.

L. Dinh, R. Pascanu, S. Bengio, and Y. Bengio. Sharp minima can generalize for deep nets. In [International Conference on Machine Learning](#), pages 1019–1028. PMLR, 2017.

P. Foret, A. Kleiner, H. Mobahi, and B. Neyshabur. Sharpness-aware minimization for efficiently improving generalization. In [International Conference on Learning Representations](#), 2021.

J. Frankle and M. Carbin. The lottery ticket hypothesis: Finding sparse, trainable neural networks. [arXiv preprint arXiv:1803.03635](#), 2018.

J. Geiping, M. Goldblum, P. E. Pope, M. Moeller, and T. Goldstein. Stochastic training is not necessary for generalization. In [International Conference on Learning Representations](#), 2022.

J. Z. HaoChen, C. Wei, J. D. Lee, and T. Ma. Shape matters: Understanding the implicit bias of the noise covariance. In [Conference on Learning Theory](#), 2021.

K. He, X. Zhang, S. Ren, and J. Sun. Deep residual learning for image recognition. In [CVPR](#), 2016.

G. Hinton, O. Vinyals, J. Dean, et al. Distilling the knowledge in a neural network. [arXiv preprint arXiv:1503.02531](#), 2(7), 2015.

T. Hoefler, D. Alistarh, T. Ben-Nun, N. Dryden, and A. Peste. Sparsity in deep learning: Pruning and growth for efficient inference and training in neural networks. [JMLR](#), 22(241):1–124, 2021.

A. Jacot, F. Gabriel, and C. Hongler. Neural tangent kernel: Convergence and generalization in neural networks. [Advances in neural information processing systems](#), 31, 2018.

A. Jacot, F. Ged, B. Şimşek, C. Hongler, and F. Gabriel. Saddle-to-saddle dynamics in deep linear networks: Small initialization training, symmetry, and sparsity. In International Conference on Machine Learning, 2021.

Z. Ji and M. Telgarsky. Directional convergence and alignment in deep learning. Advances in Neural Information Processing Systems, 33:17176–17186, 2020.

S. Kaur, J. Cohen, and Z. C. Lipton. On the maximum Hessian eigenvalue and generalization. arXiv preprint arXiv:2206.10654, 2022.

N. S. Keskar, D. Mudigere, J. Nocedal, M. Smelyanskiy, and P. T. P. Tang. On large-batch training for deep learning: Generalization gap and sharp minima. arXiv preprint arXiv:1609.04836, 2016.

A. Lewkowycz, Y. Bahri, E. Dyer, J. Sohl-Dickstein, and G. Gur-Ari. The large learning rate phase of deep learning: the catapult mechanism. arXiv preprint arXiv:2003.02218, 2020.

Q. Li, C. Tai, and E. Weinan. Stochastic modified equations and dynamics of stochastic gradient algorithms i: Mathematical foundations. The Journal of Machine Learning Research, 20(1):1474–1520, 2019a.

Y. Li, C. Wei, and T. Ma. Towards explaining the regularization effect of initial large learning rate in training neural networks. In NeurIPS, 2019b.

Z. Li, T. Wang, and S. Arora. What happens after sgd reaches zero loss?—a mathematical framework. In International Conference on Learning Representations, 2022.

K. Lyu and J. Li. Gradient descent maximizes the margin of homogeneous neural networks. In International Conference on Learning Representations, 2020.

C. Ma and L. Ying. The Sobolev regularization effect of stochastic gradient descent. arXiv preprint arXiv:2105.13462, 2021.

C. Ma, L. Wu, and L. Ying. The multiscale structure of neural network loss functions: The effect on optimization and origin. arXiv preprint arXiv:2204.11326, 2022.

E. Moroshko, B. E. Woodworth, S. Gunasekar, J. D. Lee, N. Srebro, and D. Soudry. Implicit bias in deep linear classification: Initialization scale vs training accuracy. In Advances in Neural Information Processing Systems, volume 33, pages 22182–22193, 2020.

R. Mulayoff, T. Michaeli, and D. Soudry. The implicit bias of minima stability: A view from function space. Advances in Neural Information Processing Systems, 34:17749–17761, 2021.

M. S. Nacson, K. Ravichandran, N. Srebro, and D. Soudry. Implicit bias of the step size in linear diagonal neural networks. In International Conference on Machine Learning, pages 16270–16295. PMLR, 2022.

P. Nakkiran. Learning rate annealing can provably help generalization, even for convex problems. arXiv preprint arXiv:2005.07360, 2020.

P. Nakkiran, G. Kaplun, Y. Bansal, T. Yang, B. Barak, and I. Sutskever. Deep double descent: Where bigger models and more data hurt. International Conference on Learning Representations, 2019.

S. Pesme, L. Pillaud-Vivien, and N. Flammarion. Implicit bias of sgd for diagonal linear networks: a provable benefit of stochasticity. In *Advances in Neural Information Processing Systems*, 2021.

L. Pillaud-Vivien, J. Reygner, and N. Flammarion. Label noise (stochastic) gradient descent implicitly solves the lasso for quadratic parametrisation. In *Conference on Learning Theory*, 2022.

S. L. Smith and Q. V. Le. A Bayesian perspective on generalization and stochastic gradient descent. In *International Conference on Learning Representations*, 2018.

D. Soudry, E. Hoffer, M. S. Nacson, S. Gunasekar, and N. Srebro. The implicit bias of gradient descent on separable data. *The Journal of Machine Learning Research*, 19(1):2822–2878, 2018.

T. Vaskevicius, V. Kanade, and P. Rebischini. Implicit regularization for optimal sparse recovery. *Advances in Neural Information Processing Systems*, 32, 2019.

S. Wojtowytsch. Stochastic gradient descent with noise of machine learning type. Part II: Continuous time analysis. *arXiv preprint arXiv:2106.02588*, 2021a.

S. Wojtowytsch. Stochastic gradient descent with noise of machine learning type. Part I: Discrete time analysis. *arXiv preprint arXiv:2105.01650*, 2021b.

B. Woodworth, S. Gunasekar, J. D. Lee, E. Moroshko, P. Savarese, I. Golan, D. Soudry, and N. Srebro. Kernel and rich regimes in overparametrized models. In *Proceedings of Thirty Third Conference on Learning Theory*, volume 125 of *Proceedings of Machine Learning Research*, pages 3635–3673. PMLR, 09–12 Jul 2020.

J. Wu, D. Zou, V. Braverman, and Q. Gu. Direction matters: On the implicit bias of stochastic gradient descent with moderate learning rate. *International Conference on Learning Representations*, 2021.

L. Wu, C. Ma, et al. How sgd selects the global minima in over-parameterized learning: A dynamical stability perspective. *Advances in Neural Information Processing Systems*, 31, 2018.

C. Xing, D. Arpit, C. Tsirigotis, and Y. Bengio. A walk with sgd. *arXiv preprint arXiv:1802.08770*, 2018.

C. Zhang, S. Bengio, M. Hardt, B. Recht, and O. Vinyals. Understanding deep learning requires rethinking generalization. In *International Conference on Learning Representations*, 2017.

G. Zhang, C. Wang, B. Xu, and R. Grosse. Three mechanisms of weight decay regularization. In *International Conference on Learning Representations*, 2018.

Appendix

In Section A, we show Proposition 1 and Lemma 2 on the equivalence between SGD and GD with added noise. In Section B, we provide the proof that loss stabilization occurs as written in Proposition 3. Finally, we present additional experiments in Section C.

A SGD and label noise GD

For the sake of clarity we recall below the statements of the proposition and the Lemma we prove in this section.

Proposition 5. *Let $(\theta_t)_{t \geq 0}$ follows the SGD dynamics Eq.(2) with sampling function $(i_t)_{t \geq 0}$. Define for each $t \geq 0$, the random vector $\xi_t \in \mathbb{R}^n$ such that for all $i \in \llbracket 1, n \rrbracket$,*

$$[\xi_t]_i := (h_{\theta_t}(x_i) - y_i)(1 - n\mathbf{1}_{i=i_t}). \quad (9)$$

Then, $(\theta_t)_{t \geq 0}$ follows the dynamics of the full batch gradient dynamics on \mathcal{L} where at each iteration $t \geq 0$ we inject noise ξ_t to the label vector $y \in \mathbb{R}^n$: that is at step $t \geq 0$, we compute the gradient of \mathcal{L} considering the random labels $y_t := y + \xi_t$.

Proof. Note that

$$\nabla \mathcal{L}(\theta_t) = \frac{1}{n} \sum_{i=1}^n (h_{\theta_t}(x_i) - y_i) \nabla_{\theta} h_{\theta_t}(x_i).$$

Computing the gradient considering the random labels $y_t := y + \xi_t$,

$$\nabla \widehat{\mathcal{L}}(\theta_t) = \frac{1}{n} \sum_{i=1}^n (h_{\theta_t}(x_i) - y_i - [\xi_t]_i) \nabla_{\theta} h_{\theta_t}(x_i).$$

Using $[\xi_t]_i := (h_{\theta_t}(x_i) - y_i)(1 - n\mathbf{1}_{i=i_t})$,

$$\begin{aligned} \nabla \widehat{\mathcal{L}}(\theta_t) &= \frac{1}{n} \sum_{i=1}^n (h_{\theta_t}(x_i) - y_i - (h_{\theta_t}(x_i) - y_i)(1 - n\mathbf{1}_{i=i_t})) \nabla_{\theta} h_{\theta_t}(x_i) \\ &= \sum_{i=1}^n \mathbf{1}_{i=i_t} (h_{\theta_t}(x_i) - y_i) \nabla_{\theta} h_{\theta_t}(x_i) = (h_{\theta_t}(x_{i_t}) - y_{i_t}) \nabla_{\theta} h_{\theta_t}(x_{i_t}) \end{aligned}$$

which is exactly the stochastic gradient wrt to sample (x_{i_t}, y_{i_t}) . □

Lemma 6. *For $t \geq 0$, let $\xi_t \in \mathbb{R}^n$ be defined as above, then ξ_t is a mean zero random vector with variance such that $\frac{1}{n(n-1)} \mathbb{E} \|\xi_t\|^2 = 2\mathcal{L}(\theta_t)$.*

Proof. Recall that, for all $i \leq n$, we have $[\xi_t]_i = (h_{\theta_t}(x_i) - y_i)(1 - n\mathbf{1}_{i=i_t})$, where $i_t \sim \mathcal{U}(\llbracket 1, n \rrbracket)$. Now taking the expectation,

$$\mathbb{E}[\xi_t]_i = \mathbb{E}[(h_{\theta_t}(x_i) - y_i)(1 - n\mathbf{1}_{i=i_t})] = (h_{\theta_t}(x_i) - y_i)(1 - n\mathbb{E}[\mathbf{1}_{i=i_t}]) = 0,$$

as $\mathbb{E}[\mathbf{1}_{i=i_t}] = 1/n$. Coming to the variance,

$$\begin{aligned}
\mathbb{E} \|\xi_t\|^2 &= \mathbb{E} \left[\sum_{i=1}^n [\xi_t]_i^2 \right] = \sum_{i=1}^n \mathbb{E} [\xi_t]_i^2 \\
&= \sum_{i=1}^n (h_{\theta_t}(x_i) - y_i)^2 \mathbb{E} [(1 - n\mathbf{1}_{i=i_t})^2] \\
&= \sum_{i=1}^n (h_{\theta_t}(x_i) - y_i)^2 \mathbb{E} [(1 - 2n\mathbf{1}_{i=i_t} + n^2\mathbf{1}_{i=i_t})] \\
&= \sum_{i=1}^n (h_{\theta_t}(x_i) - y_i)^2 (1 - 2 + n) \\
&= (n-1) \sum_{i=1}^n (h_{\theta_t}(x_i) - y_i)^2 \\
&= 2n(n-1)\mathcal{L}(\theta_t),
\end{aligned}$$

and this concludes the proof of the lemma. \square

B Quadratic parameterization in one dimension

Again, for the Appendix to be self-contained, we recall the setup of the Proposition 3 on loss stabilization. We consider a regression problem with quadratic parameterization on one-dimensional data inputs x_i 's, coming from a distribution $\hat{\rho}$, and outputs generated by the linear model $y_i = x_i\theta_*^2$. The loss writes $F(\theta) := \frac{1}{4}\mathbb{E}_{\hat{\rho}}(y - x\theta^2)^2$, and the SGD iterates with step size $\eta > 0$ follow, for any $t \in \mathbb{N}$,

$$\theta_{t+1} = \theta_t + \eta \theta_t x_{i_t} (y_{i_t} - x_{i_t} \theta_t^2) \quad \text{where} \quad x_{i_t} \sim \hat{\rho}. \quad (10)$$

We rewrite the proposition here.

Proposition 7. *Assume $\exists x_{\min}, x_{\max} > 0$ such that $\text{supp}(\hat{\rho}) \subset [x_{\min}, x_{\max}]$. Then for any $\eta \in ((\theta_* x_{\min})^{-2}, 1.25(\theta_* x_{\max})^{-2})$, any initialization in $\theta_0 \in (0, \theta_*)$, for $t \in \mathbb{N}$, we have almost surely*

$$F(\theta_t) \in (\epsilon_o^2 \theta_*^2, 0.17 \theta_*^2). \quad (11)$$

where $\epsilon_o = \min \{(\eta(\theta_* x_{\min})^2 - 1)/3, 0.02\}$. Also, almost surely, there exists $t, k > 0$ such that $\theta_{t+2k} \in (0.65 \theta_*, (1 - \epsilon_o) \theta_*)$ and $\theta_{t+2k+1} \in ((1 + \epsilon_o) \theta_*, 1.162 \theta_*)$.

Proof. Consider SGD recursion Eq.(10) and note that $y = x\theta_*^2$.

$$\begin{aligned}
\theta_{t+1} &= \theta_t + \eta \theta_t x (x\theta_*^2 - x\theta_t^2) \\
\theta_{t+1} &= \theta_t + \eta \theta_t x^2 (\theta_*^2 - \theta_t^2)
\end{aligned}$$

For the clarity of exposition, we consider the rescaled recursion of the original SGD recursion.

$$\theta_{t+1}/\theta_* = \theta_t/\theta_* + \eta \theta_*^2 x^2 \theta_t/\theta_* \left(1 - (\theta_t/\theta_*)^2\right),$$

and, by making the benign change $\theta_t \leftarrow \theta_t/\theta_*$, we focus on the stochastic recursion instead,

$$\theta_{t+1} = \theta_t + \gamma\theta_t(1 - \theta_t^2), \quad (12)$$

where $\gamma \sim \hat{\rho}_\gamma$ the pushforward of $\hat{\rho}$ under the application $z \rightarrow \eta\theta_*^2 z^2$. Let $\Gamma := \text{supp}(\hat{\rho}_\gamma)$, the support of the distribution of γ . From the range of η , it can be verified that $\Gamma \subseteq (1, 1.25)$. Now the proof of the theorem follows from Lemma 9. \square

Lemma 8 (Bounded Region). *Consider the recursion Eq.(12), for $\Gamma \subseteq (1, 1.25)$ and $0 < \theta_0 < 1$, then for all $t > 0$, $\theta_t \in (0, 1.162)$.*

Proof. Consider a single step of Eq.(12), for some $\gamma \in (1, 1.25)$,

$$\theta_+ = \theta + \gamma\theta(1 - \theta^2)$$

The aim is to show that θ_+ stays in the interval $(0, 1.162)$. In order to show this, we do a casewise analysis.

For $\theta \in (0, 1]$: Since $0 < \theta \leq 1$, we have $\theta_+ \geq \theta > 0$. To prove the bound above, consider the following quantity,

$$\theta_{max} = \max_{\gamma \in (1, 1.25)} \max_{\theta \in (0, 1]} \theta + \gamma\theta(1 - \theta^2) \quad (13)$$

Say $h_\gamma(\theta) = \theta + \gamma\theta(1 - \theta^2)$, note that $h'_\gamma(\theta) = 1 + \gamma - 3\gamma\theta^2$ and $h''_\gamma(\theta) = -6\gamma\theta < 0$. Hence, for any γ in our domain, the maximum is attained at $\theta_\gamma = \frac{1}{\sqrt{3}}\sqrt{\frac{1}{\gamma} + 1}$ and $h_\gamma(\theta_\gamma) = \frac{2(1+\gamma)^{3/2}}{3\sqrt{3\gamma}}$.

$$\max_{\gamma \in (1, 1.25)} \max_{\theta \in (0, 1]} \theta + \gamma\theta(1 - \theta^2) = \max_{\gamma \in (1, 1.25)} \frac{2(1+\gamma)^{3/2}}{3\sqrt{3\gamma}}$$

It can be verified that $\frac{2(1+\gamma)^{3/2}}{3\sqrt{3\gamma}}$ is increasing with gamma in the interval $(1, 1.25)$. Hence,

$$\max_{\gamma \in (1, 1.25)} \frac{2(1+\gamma)^{3/2}}{3\sqrt{3\gamma}} \leq \left. \frac{2(1+\gamma)^{3/2}}{3\sqrt{3\gamma}} \right|_{\gamma=1.25} < 1.162 \quad (14)$$

Combining them, we get,

$$\theta_+ \leq \max_{\gamma \in (1, 1.25)} \max_{\theta \in (0, 1]} \theta + \gamma\theta(1 - \theta^2) < 1.162 \quad (15)$$

For $\theta \in (1, 1.162]$: Since $\theta > 1$, we have, $\theta_+ < \theta < 1.162$. For lower bound, note that for θ_+ to be less than 0, we need $1 + \gamma - \gamma\theta^2 < 0$. But for $\gamma \in (1, 1.25)$ and $\theta \in (1, 1.162)$,

$$\gamma(\theta^2 - 1) < 1.25((1.162)^2 - 1) < 1.$$

Hence, it never goes below 0. \square

Lemma 9. *Consider the recursion Eq.(12) with $\Gamma \subseteq (1, 1.25)$ and θ_0 initialized uniformly in $(0, 1)$. Then, there exists $\epsilon_0 > 0$, such that for all $\epsilon < \epsilon_0$ there exists $t > 0$ such that for any $k > 0$,*

$$\theta_{t+2k} \in (0.65, 1 - \epsilon) \quad \text{and} \quad \theta_{t+2k+1} \in (1 + \epsilon, 1.162)$$

almost surely.

Proof. Define $\gamma_{\min} > 1$ as the infimum of the support Γ . Let $\epsilon_o = \min\{(\gamma_{\min}-1)/3, 0.02\}$. Note that $\epsilon_0 > 0$ as $\gamma_{\min} > 1$. Now for any $0 < \epsilon < \epsilon_o$, we have $\gamma_{\min}(2-\epsilon)(1-\epsilon) > 2$.

Divide the interval $(0, 1.162)$ into 4 regions, $I_0 = (0, 0.65]$, $I_1 = (0.65, 1-\epsilon)$, $I_2 = [1-\epsilon, 1)$, $I_3 = (1, 1.162)$. The strategy of the proof is that the iterates will eventually end up in I_1 and that once it ends up in I_1 , it comes back to I_1 in 2 steps.

Let θ_0 be initialized uniformly random in $(0, 1)$. Consider the sequence $(\theta_t)_{t \geq 0}$ generated by

$$\theta_{t+1} = h_{\gamma_t}(\theta_t) := \theta_t + \gamma_t \theta_t(1 - \theta_t^2) \quad \text{where} \quad \gamma_t \sim \hat{\rho}_\gamma. \quad (16)$$

We prove the following facts **(P1)-(P4)**:

(P1) There exists $t \geq 0$ such that the $\theta_t \in I_1 \cup I_2 \cup I_3$.

(P2) Let $\theta_t \in I_3$, then $\theta_{t+1} \in I_1 \cup I_2$.

(P3) Let $\theta_t \in I_2$, there exists $k > 0$ such that for $k' < k$, $\theta_{t+2k'} \in I_2$ and $\theta_{t+2k} \in I_1$.

(P4) When $\theta_t \in I_1$, then for all $k \geq 0$, $\theta_{t+2k} \in I_1$ and $\theta_{t+2k+1} \in (1+\epsilon, 1.162)$.

Proof of (P1)-(P4): Let $t \in \mathbb{N}$, note first that the event $\{\theta_t = 1\} = \cup_{k \leq t} \{\theta_k = 1 | \theta_{k-1} \neq 1\}$ and hence a finite union of zero measure sets. Hence $\{\theta_t = 1\}$ is a zero measure set and therefore we do not consider it below. For any other sequence, from the above four properties, we can conclude that the lemma holds.

Proof of P1: Assume that until time $t > 0$, the iterates are all in I_0 , then we have

$$\theta_t = \theta_{t-1}(1 + \gamma(1 - \theta_{t-1}^2)) \geq \theta_{t-1}(2 - \theta_{t-1}^2) > 1.5 \theta_{t-1} > 1.5^t \theta_0$$

Hence, the sequence eventually exits I_0 . We know that it will stay bounded from Lemma 8, hence it will end up in $I_1 \cup I_2 \cup I_3$.

Proof of P2: For any $\theta_t \in (1, 1.162)$, $1 < \gamma < 1.25$, since $h_\gamma(\cdot)$ is decreasing in $(1, 1.162)$, we have $h_\gamma(1.162) < h_\gamma(\theta_t) < h_\gamma(1)$. Also $h_\gamma(\theta)$ is linear in gamma with negative coefficient for $\theta > 1$. Hence it decreases as γ increases. Using this,

$$.652 = h_{1.25}(1.162) < h_\gamma(1.162) < h_\gamma(\theta_t) < h_\gamma(1) = 1.$$

Hence, $\theta_{t+1} \in I_1 \cup I_2$.

Proof of P3: The proof of this follows from Lemma 11.

Proof of P4: The proof of this follows from Lemma 14. □

Lemma 10. For any $\theta \in I_1 \cup I_2$ and any $a, b \in \Gamma$, $h_a(h_b(\theta)) \in I_1 \cup I_2$,

$$h_{\gamma_{\max}}(h_{\gamma_{\max}}(\theta)) \leq h_a(h_b(\theta)) \leq h_{\gamma_{\min}}(h_{\gamma_{\min}}(\theta)). \quad (17)$$

Proof. For any $\gamma \in \Gamma$, recall

$$h_\gamma(\theta) = \theta + \gamma \theta(1 - \theta^2) = 1 + (1 - \theta)(\gamma \theta(1 + \theta) - 1)$$

Note that for $\theta \in I_1 \cup I_2$, $\theta(1 + \theta) > 1$, Hence $\gamma \theta(1 + \theta) > 1$. This gives us that $h_\gamma(\theta) > 1$. Now we will track where $\theta \in I_1 \cup I_2$ can end up after two stochastic gradient steps.

- For any $b \in \Gamma$, as $\theta \in I_1 \cup I_2$, we have

$$h_{\gamma_{\max}}(\theta) \geq h_b(\theta) \geq h_{\gamma_{\min}}(\theta) > 1,$$

note $h_{\gamma_{\max}}(\theta) \geq h_b(\theta) \geq h_{\gamma_{\min}}(\theta)$ holds since $\theta < 1$.

- Now for any $a \in \Gamma$ and $x > 1$, $h_a(x)$ is a decreasing function in x . Hence

$$h_a(h_{\gamma_{\max}}(\theta)) \leq h_a(h_b(\theta)) \leq h_a(h_{\gamma_{\min}}(\theta)).$$

Using $\gamma_{\min} \leq a$, $h_a(h_{\gamma_{\min}}(\theta)) \leq h_{\gamma_{\min}}(h_{\gamma_{\min}}(\theta))$, Similarly using $\gamma_{\max} > a$, we have, $h_{\gamma_{\max}}(h_{\gamma_{\max}}(\theta)) \leq h_a(h_{\gamma_{\max}}(\theta))$. Combining them we get,

$$h_{\gamma_{\max}}(h_{\gamma_{\max}}(\theta)) \leq h_a(h_b(\theta)) \leq h_{\gamma_{\min}}(h_{\gamma_{\min}}(\theta)). \quad (18)$$

Similar argument can extend it to,

$$h_{1.25}(h_{1.25}(\theta)) < h_a(h_b(\theta)) < h_1(h_1(\theta)). \quad (19)$$

□

Lemma 11. *Let $\theta_t \in I_2$, there exists $k > 0$ such that $\theta_{t+2k} \in I_1$.*

Proof. For any $\gamma \in \Gamma$, let $\theta_+ = h_\gamma(\theta)$, then we have

$$h_\gamma(h_\gamma(\theta)) - \theta = h_\gamma(\theta_+) - \theta = \gamma\theta(1 - \theta^2) + \gamma\theta_+(1 - \theta_+^2).$$

Furthermore,

$$\begin{aligned} \theta_+ &= \theta + \gamma\theta(1 - \theta^2) = \theta(1 + \gamma(1 - \theta^2)), \\ 1 + \theta_+ &= 1 + \theta + \gamma\theta(1 - \theta^2) = (1 + \theta)(1 + \gamma\theta(1 - \theta)), \\ 1 - \theta_+ &= 1 - \theta - \gamma\theta(1 - \theta^2) = (1 - \theta)(1 - \gamma\theta(1 + \theta)). \end{aligned}$$

And multiplying the above three terms and adding $\theta(1 - \theta^2)$, we get,

$$\theta_+(1 - \theta_+^2) + \theta(1 - \theta^2) = \theta(1 - \theta^2) \{ 1 + \underbrace{[(1 + \gamma(1 - \theta^2))(1 + \gamma\theta(1 - \theta))(1 - \gamma\theta(1 + \theta))]}_{P(\theta)} \}$$

For $\theta \in I_2$, using $\gamma_{\min}(2 - \epsilon)(1 - \epsilon) > 2$, we have the inequalities

$$\begin{aligned} (1 + \gamma(1 - \theta^2))(1 + \gamma\theta(1 - \theta)) &> 1, \\ (1 - \gamma\theta(1 + \theta)) &< 1 - \gamma_{\min}(2 - \epsilon)(1 - \epsilon) < -1, \\ P(\theta) &< -1. \end{aligned}$$

Hence,

$$h_\gamma(h_\gamma(\theta)) - \theta = \gamma(1 - \theta^2)(1 + P(\theta)) < 0. \quad (20)$$

Therefore, for $[1 - \epsilon, 1]$, for any $\gamma \in \Gamma$, $h_\gamma(h_\gamma(\theta)) < \theta$. Hence for any two stochastic gradient step with $a, b \in \Gamma$, from Eq.(17), $\theta_{t+2} = h_a(h_b(\theta_t)) \leq h_{\gamma_{\min}}(h_{\gamma_{\min}}(\theta_t)) < \theta_t$. From any point in I_2 , we have $|\theta_{t+2} - 1| > |\theta_t - 1|$, for any $a, b \in \Gamma$. Intuitively this means that in *two gradient steps* the iterates move *further away from 1* until it eventually leaves the interval I_2 as the sequence $\{\theta_{t+2k}\}_{k \geq 0}$ is strictly decreasing with no limit point in I_2 . From Lemma 13, we know that in two steps the iterates will never leave $I_1 \cup I_2$. Hence they will eventually end up in I_1 leaving I_2 . □

Property 12. Define $g_\gamma(\theta) := h_\gamma(h_\gamma(\theta))$ for the sake of brevity. The followings properties hold for $\theta \in I_1 \cup I_2$, $\gamma \in \Gamma$ and θ_γ the root of $h'_\gamma(\theta)$:

Q1 $g_\gamma(\theta) \geq g_\gamma(\theta_\gamma)$.

Q2 The function $g_\gamma(\cdot)$ is decreasing in $[0.65, \theta_\gamma]$ and increasing in $(\theta_\gamma, 1]$.

Proof. Note $h'_\gamma(\theta) = 1 + \gamma - \gamma 3\theta^2$ has at most one root $\theta_\gamma \in (0, 1)$. Note that for all $\gamma \in \Gamma$, $\theta_\gamma \in I_1 \cup I_2$. For any γ , $g'_\gamma(\theta) = h'_\gamma(h_\gamma(\theta))h'_\gamma(\theta)$. For any $\theta \in I_1 \cup I_2$, we have, $h_\gamma(\theta) > 1 \implies h'_\gamma(h_\gamma(\theta)) < 0$. Therefore, $g'_\gamma(\theta)$ has only one root in $I_1 \cup I_2$. Since $\theta_\gamma \in I_1 \cup I_2$, note $g''_\gamma(\theta_\gamma) = h'_\gamma(h_\gamma(\theta_\gamma))h''_\gamma(\theta_\gamma) > 0$. Therefore, $g_\gamma(\cdot)$ attains its minimum at θ_γ and this shows the desired properties. \square

Lemma 13. For any $\theta \in I_1 \cup I_2$ and any $a, b \in \Gamma$, $h_a(h_b(\theta)) \in I_1 \cup I_2$.

Proof. **Lower Bound:** From Eq.(19), we know

$$h_{1.25}(h_{1.25}(\theta)) < h_a(h_b(\theta))$$

We know that from property **Q1** that $g_\gamma(\theta) \geq g_\gamma(\theta_\gamma)$. Hence

$$g_{1.25}(\theta_{1.25}) < g_{1.25}(\theta) < h_a(h_b(\theta))$$

It can be quickly checked that $.65 < g_{1.25}(\theta_{1.25})$. Hence the lower bound holds.

Upper Bound: From Eq.(19), we know

$$h_a(h_b(\theta)) < h_1(h_1(\theta))$$

We know that from property **Q2** that $g_1(\theta) \leq \max\{g_1(1), g_1(0.65)\}$. It can be easily verified that $g_1(0.65) < 0.98$. Hence $g_1(\theta) < 1$.

\square

Lemma 14. For any $\theta \in I_1$ and any $a, b \in \Gamma$, $h_a(h_b(\theta)) \in I_1$ and $h_a(\theta) \in (1 + \epsilon, 1.162)$.

Proof. The lower bound in Lemma 13 holds here. For the upper bound, from and Eq.(17),

$$h_a(h_b(\theta)) \leq h_{\gamma_{\min}}(h_{\gamma_{\min}}(\theta))$$

Using property **Q2**,

$$h_{\gamma_{\min}}(h_{\gamma_{\min}}(\theta)) \leq \max\{g_{\gamma_{\min}}(1 - \epsilon), g_{\gamma_{\min}}(0.65)\}$$

From Eq.(20), $g_{\gamma_{\min}}(1 - \epsilon) < 1 - \epsilon$. From Eq.(19), $g_{\gamma_{\min}}(0.65) < g_1(0.65) < 0.98 < 1 - \epsilon$. In I_1 , the function $h_a(\cdot)$ first increases reaches maximum and decreases. Hence for $\theta \in I_1$, $h_a(\theta) \geq \min\{h_a(0.65), h_a(1 - \epsilon)\}$.

$$\begin{aligned} h_a(1 - \epsilon) &\geq 1 - \epsilon + a(1 - (1 - \epsilon)^2)(1 - \epsilon), \\ &= 1 - \epsilon + a(2\epsilon - \epsilon^2)(1 - \epsilon), \\ &\geq 1 - \epsilon + \gamma_{\min}(2\epsilon - \epsilon^2)(1 - \epsilon), \\ &= 1 + \epsilon + \epsilon(\gamma_{\min}(2 - \epsilon)(1 - \epsilon) - 2) > 1 + \epsilon. \end{aligned}$$

Also $h_a(0.65) > h_1(0.65) > 1.02 > 1 + \epsilon$, therefore $h_a(\theta) > 1 + \epsilon$ and this completes the proof. \square

C Additional experimental results

This section of the appendix presents additional experiments complementing the ones presented in the main text. To give a short overview of their content, here is a formal description. More details can be found in the captions.

- Figure 8 shows that even if loss stabilization occurs in diagonal linear networks, the implicit bias towards sparsity is largely weaker than that of SGD and generalization is poor.
- Figures 9 and 10 demonstrate that the implicit bias resulting from high-loss stabilization makes the neural nets learn *first* a simple model *then eventually* fits the data.
- Figure 11 presents the sparsifying effect corresponding to the neurons' movements exhibited in Figure 5.
- Figure 12 showcases the features learning induced by large step sizes for different layers of ResNets-18 when trained on CIFAR-10.
- Figures 13 and 14 exhibit the feature sparsity in ResNets architecture on CIFAR-10 and CIFAR-100 without any regularization (plain SGD) and in the state-of-the-art setup.

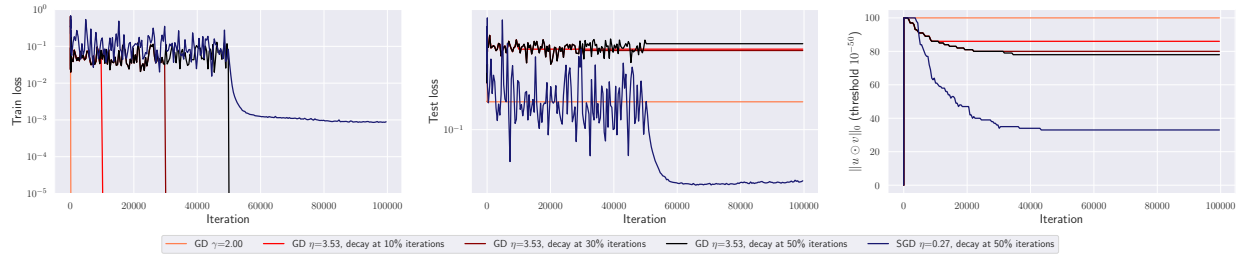


Figure 8: Diagonal linear networks. Loss stabilization also occurs for *full-batch gradient descent* but does not lead to a similar level of sparsity as SGD and also does not improve the test loss.

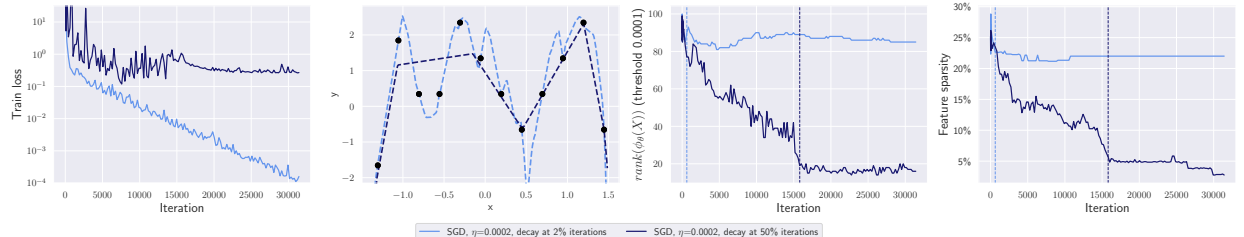


Figure 9: Two-layer ReLU networks for 1D regression. Unlike for Fig. 4, here we use a larger warmup coefficient ($500\times$ vs. $400\times$) which leads to overregularization such that the 50%-schedule run fails to fit all the training points and gets stuck at a too high value of the training loss ($\approx 10^{-0.5}$).

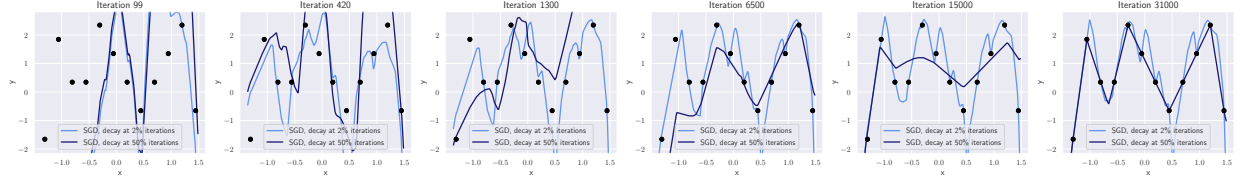


Figure 10: Two-layer ReLU networks for 1D regression. Illustration of the resulting models from Fig. 4 over training iterations. We can see that first the model is simplified and only then it fits the training data.

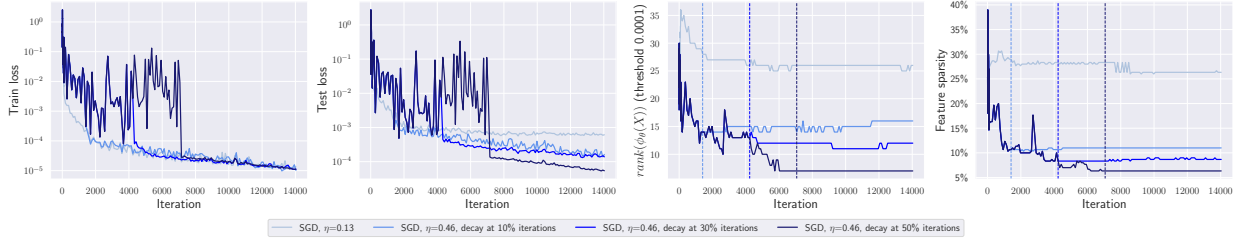


Figure 11: Two-layer ReLU networks in a teacher-student setup. Loss stabilization for two-layer ReLU nets in the teacher-student setup with input dimension $d = 2$. We observe loss stabilization, better test loss for longer schedules and sparser features due to simplification of $\phi(X)$.

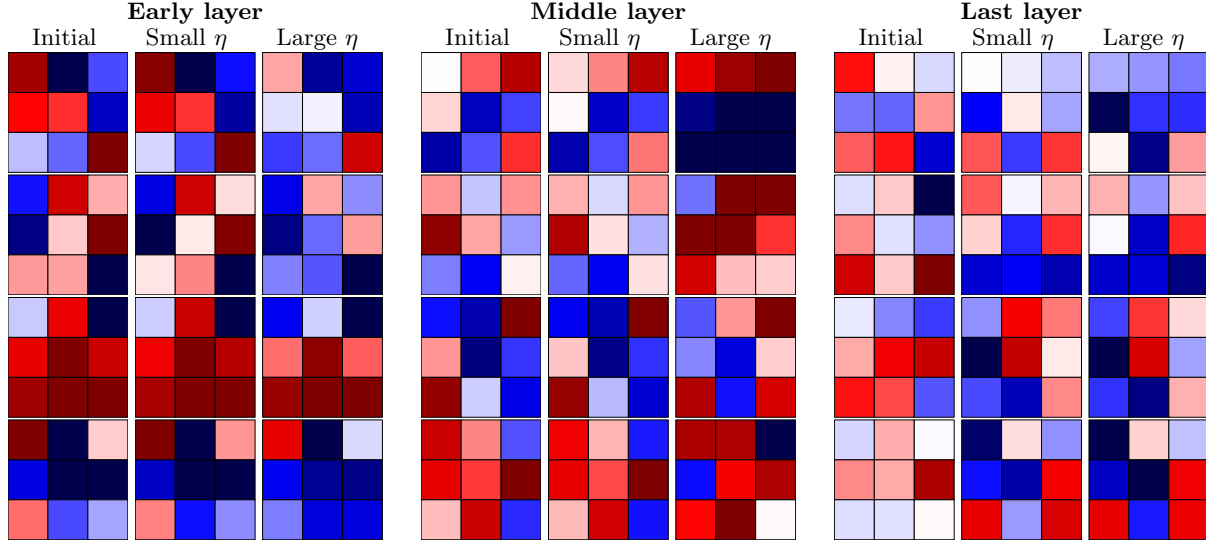
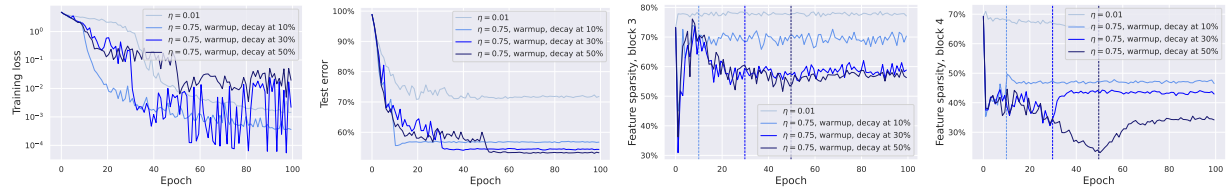


Figure 12: Visualization on four sets of convolutional filters taken from different layers of ResNets-18 trained on CIFAR-10 with small vs. large step size η (the 50% decay schedule). For small step sizes, the early and middle layers stay very close to randomly initialized ones which indicates the absence of feature learning.

ResNet-34 on CIFAR-100, no explicit regularization



ResNet-34 on CIFAR-100, state-of-the-art setting

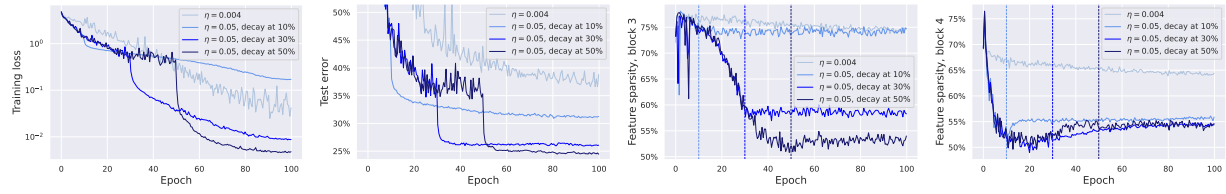


Figure 13: ResNet-34 trained on CIFAR-100. Both *without explicit regularization* and in the *state-of-the-art setting*, the training loss stabilizes, the test loss significantly depends on the length of the schedule, and feature sparsity is minimized over iterations. However, differently from the plots on CIFAR-10, here without explicit regularization we observe oscillating behavior after the step size decay (although at a very low level between 10^{-4} and 10^{-2}).

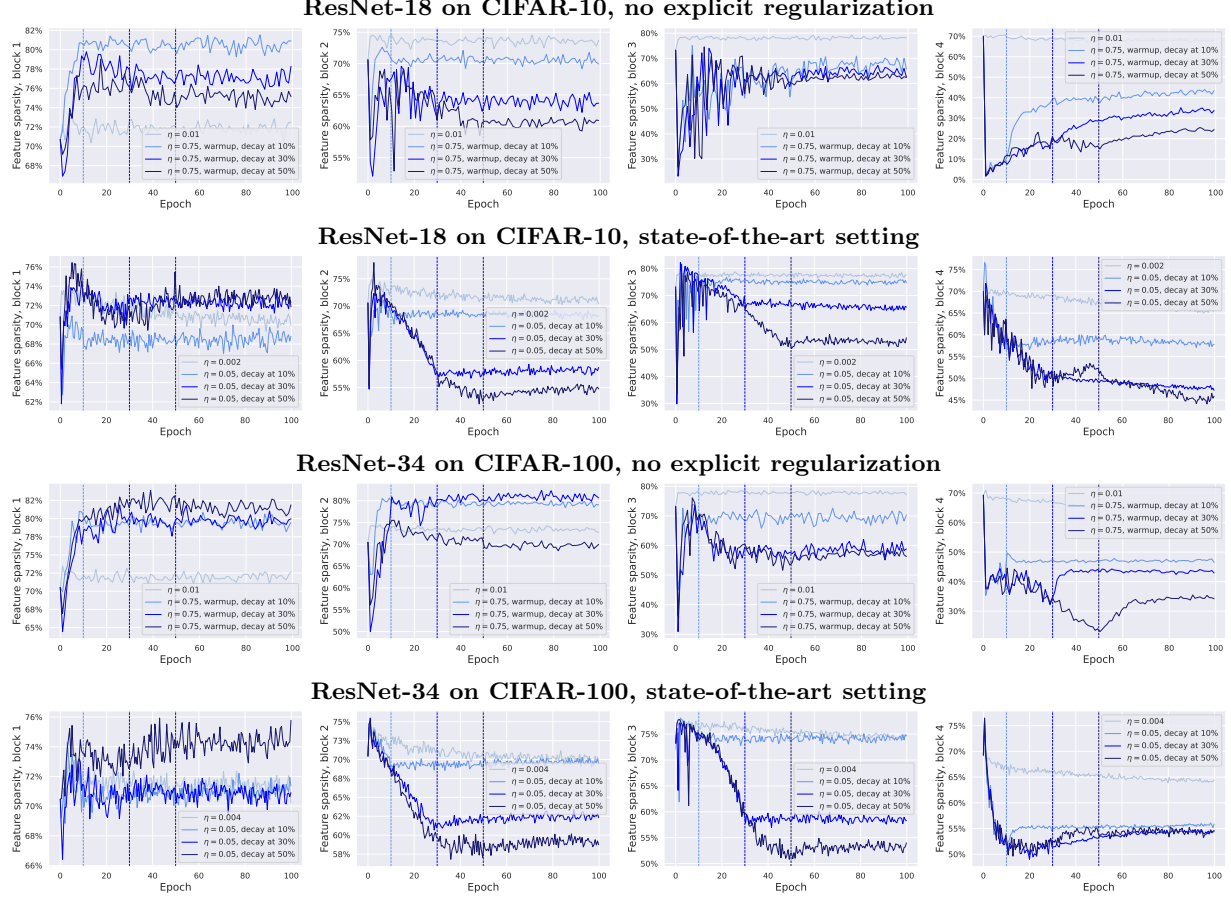


Figure 14: Feature sparsity for ResNets on CIFAR-10 and CIFAR-100. Compared to the previous figures, here we additionally show it for the first and second super-blocks. We can see that large step size schedules consistently lead to a much lower sparsity at super-blocks 3 and 4. In 3 out of 4 models the sparsity is lower at super-block 2 as well. However, for super-block 1, there is no clear trend between different training methods.